Year-round performance assessment of a ground source heat pump with multiple energy piles

Yuanlong Cui, Jie Zhu*

Department of Architecture and Built Environment

The University of Nottingham, University Park, Nottingham NG7 2RD, United Kingdom

ABSTRACT

The year-round performance of a ground source heat pump (GSHP) with multiple energy piles (EPs) is investigated in this study based on a 3D transient heat transfer model. The GSHP heating and cooling capabilities are simulated and assessed according to thermal energy demands of an air conditioned domestic building, its coefficients of performance (COPs) obtained from numerical analyses and experimental tests are compared and the largest difference between them is less than 8%. The maximum heating and cooling COPs of the GSHP are 3.63 and 4.73 respectively in the first year operation period, and the soil final temperature is lower than its initial temperature, therefore the soil is not capable of recovering by itself due to the building unbalanced heating and cooling loads. Finally, the effects of the soil thermal properties on its temperature and the GSHP COPs are investigated and compared between the first year and tenth year operations, and it is found that the soil with low volumetric heat capacity and high thermal conductivity could achieve a quick temperature recovery.

Keywords: Energy piles, GSHP, Ground heat extraction/injection, Soil thermal property, COPs

1 Introduction

Shallow geothermal energy is one of the most popular renewable energy sources for efficient building air conditioning with GSHP. A typical GSHP system is presented in Fig.1, which consists of three main components: (i) ground heat exchanger (GHE), (ii) heat pump and (iii) ventilation system [1]. In winter, soil temperature is higher than the mean ambient air temperature, and therefore the soil can be used as a heat source for space heating; however, in summer, its temperature is lower than the average outdoor air's and the soil can be adopted as a heat sink for space cooling. Thereby soil temperature is a very important parameter and should be clarified for designing GHE, which is decided by the geographic location and regional climate condition. Numerous

* Corresponding author. Tel: +44-115-8466141 Fax: +44-115-951315
E-mail address: jie.zhu@nottingham.ac.uk

approaches have been developed to predict soil temperature, such as numerical [2, 3], analytical and semi-empirical [4-5], statistical and purely empirical methods [6]. Mihalakakou et al. [2] proposed a 3D transient numerical heat transfer model to assess the soil temperatures at different depths under a building foundation, and got a very good agreement between numerical results and measurement data, the maximum soil temperature difference between them is less than 0.3 °C. Zoras et.al [3] developed a numerical response factor method to simulate soil temperature variation under a normal square slab-on-ground floor, and found that the method precision relies on the depth of grid nodes regarding the time required for heat waves to penetrate at their locations. Droulia et al. [4] calculated the subsurface soil temperature profile based on analytical and semi-empirical models, and discovered that the semi-analytical approach only needs daily mean soil or air temperature, while the analytical solution does not require any data at all. Elias et al. [5] studied soil temperature distribution by an exponential-sinusoidal analytical model and compared their results with the analytical solution data, and found that the maximum soil temperature error is 0.3 °C at a depth of 0.1 m. Zheng et al. [6] presented a normal methodology to calculate daily soil temperature based on the ambient air temperature and precipitation statistical data, and examined soil temperature distribution under vegetation cover by the Leaf Area Index (LAI). Their results demonstrate that soil temperature under vegetation cover at regional and continental scales can be decided through LAI. It is essential to sustain high soil temperature surrounding the GHE for good performance, so several techniques are adopted to manipulate geothermal energy system design based on theoretical models [7-9]. Li and Lai [10] developed analytical model targeting on heat conduction in infinite anisotropic and semi-infinite media, and concluded that the anisotropy of the medium has little impact on the short time performance of GHE, while it has obvious effect on the long-term temperature response. Notably, soil thermal property is another vital factor affecting ground heat transfer. Casasso and Sethi [11] descripted that soil thermal conductivity is a key source of uncertainty when modelling the GSHPs. Their results reveal that a fluid temperature difference of 5.66 °C and heat pump energy consumption difference of 12.5% exist for soil thermal conductivity difference of 1.5 W/(m·K). Lee [12] studied the impact of vertical heterogeneities of the soil thermal conductivity, and found that the adoption of depth-averaged thermal parameters is appropriate.

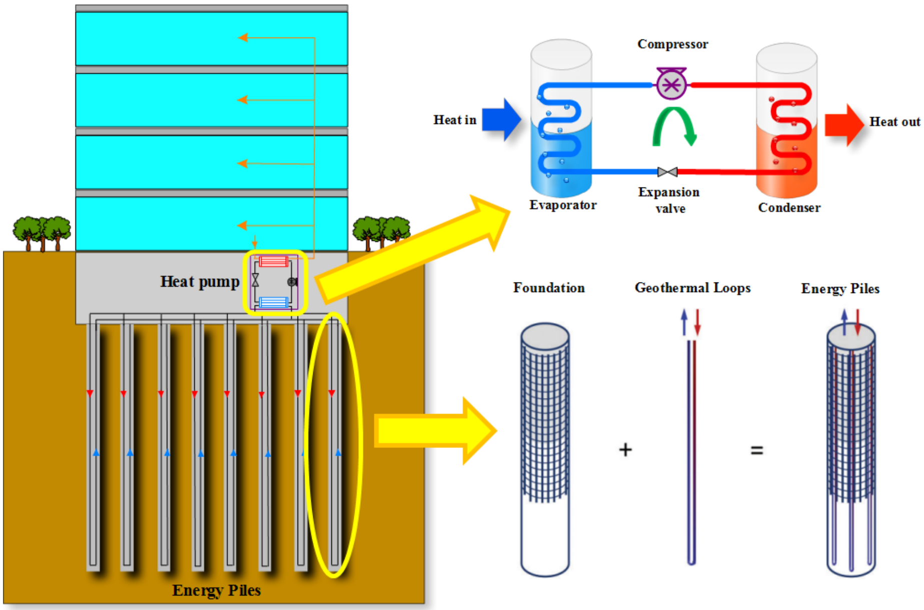

Fig. 1. A typical GSHP system [1].

The amount of heat extracted/rejected from/to the soil in the GSHP system relies on building heating/cooling load. Correspondingly, the GHE should have the ability to meet the building thermal energy requirement. Over the years, various analytical and numerical vertical GHE models have been proposed and utilized as the design tools, which are also used to estimate the working fluid temperature in the GHE for thermal performance evaluation. Moch et al. [13] developed two 2D axisymmetric analytical models to analyse thermal interaction between the soil and a helical BHE, and found that thermal properties of the soil have a significant influence on sizing the geothermal installation. Al-Khoury et al. [14-16] proposed a 3D numerical model depicting thermal interactions among inlet-pipe, outlet-pipe and grout. Their model addresses the formulation equilibrium, effects of thermal resistance and finite element method (FEM) discretization. Ozudogru et al. [17] suggested a 3D numerical model for vertical GHE based on FEM for simulating two cases, namely, an EP with double U-tubes and a BHE with a single U-tube, and demonstrated that the model can be successfully used to predict vertical BHE and EPs performances with different sizes and loop configurations.

Recently, EPs have received more attention, because a GSHP with EPs is one of the most effective strategies for building air conditioning [18, 19], thereby a number of research works have been implemented on its thermal characteristics [20-24]. Olgun et al. [1] analysed 30-year operation characteristics of EPs to evaluate the long-term performance with balanced and unbalanced heating loads under different climatic conditions, and discovered temperature variation of the soil surrounding an EP mainly depends on the seasonal energy requirement. Gashti et al. [25] proposed a 3D numerical heat transfer model based on finite element theory to assess the performance of steel pile foundations by Comsol Multiphysics package. Their study results show that temperature difference between the pile wall and inlet fluid is around 25–33%, and there is a big temperature fluctuation near the tube curve at the EP end. Li et al. [26] simulated the soil temperature surrounding an EP, and deduced that the influence of pile thermal load on the soil temperature decreases with radial distance. Capozza et al. [27] investigated the long-term and seasonal behaviours of a GSHP unit by CaRM simulation tool to figure out unbalanced thermal load profiles for two office buildings in Italy, and found that the soil temperature depends mainly on the annual heating and cooling loads. Kim et al. [28] used TRNSYS program to assess the performance of a GSHP system with vertical BHEs, and discovered that the COPs of heating and cooling could be individually improved by up to 25.2% and 15.1% with a systematic approach. Darkwa et al. [29] studied the long-term performance of a single BHE, and presented that the yearly mean thermal energy rejected into the BHE is approximately 4.5 times more than the amount extracted. Pasquier and Marcotte [30] developed a quasi-3D numerical model for a single BHE as well, and considered thermal capacitances of both the grouting material and working fluid. Their results illustrate that the error of the working fluid temperature is lower than the measurement uncertainty. Retkowski and Thöming [31] presented a mixed-integer nonlinear programming method to minimize the year-round running cost of vertical BHE system, but thermal interaction between BHEs is not considered. Lee et al. [32] compared the transient performance features between a hybrid GSHP using a heat storage bath and a pure one, and found that the mean COP of the hybrid GSHP system is around 7.2% higher than that of the pure one at the optimum operating condition. Kurevija et al. [33] analysed the long-term thermal disturbance between boreholes in Zagreb using the g-functions, and adopted a constant energy efficiency for heat pump unit. Ghoubali et al. [34] investigated a heat pump performance with simultaneous domestic hot water heating, space heating and cooling functions using TRNSYS software under three different weather conditions in France, and a maximum seasonal COP of 2.28 is achieved. Kizilkan and Dincer [35] deduced exergy and energy assessments of a GSHP system in Ontario, Canada, and found that the system performance in cooling mode is slightly lower than that in heating mode. Zhao et al. [36] developed a 3D transient model to investigate thermal behaviours of different GHEs, such as, U-shaped, W-shaped and spiral-shaped. Their numerical results present that the spiral-shaped GHE provides the lowest temperature working fluid under the same initial and boundary conditions. Luo et al. [37] carried out numerical and experimental studies of a GSHP with four different kinds of GHEs including double-U, triple-U, double-W and spiral-shaped under an intermittent operating condition, and found that the double-U type has the lowest energy performance and its thermal efficiency only accounts for 67~69% that of the spiral or double-W category. Hamada et al. [38] studied the field performance of a GSHP with EP system, and discovered that the system heat output accounts for around 90% of the predicated value and the mean COP for space heating is 3.9.

Currently, there is a need to fill the research gap in studying the multiple EPs year-round performance with consideration of "thermal short-circuiting" and soil thermal property effects, even though few mathematical models focusing on heat transfer in the shallow EPs have been produced. The objectives of this paper are to investigate the year-round performance of a GSHP with multiple EPs and identify the influence of soil thermal property. In this study, a 3D numerical model is used to discretize the EP components and working fluid along the U-tube pipe for accurate representation of heat transfer procedure, heat extraction and injection capacities are calculated through C code.

2 Numerical model

An existing 3D transient heat transfer numerical model based on finite volume method (FVM) [39] is adopted in this study, the effect of "thermal short-circulating" between two pipes of a U-tube in EP is taken into account, and the initial and boundary conditions are established. Thermal partial differential equations of the model are discretized at spatial nodal points and solved by linear approximation method. The major elements in heat transfer process are the nearby soil, concrete piles, polyethylene U-tube pipes and working fluid. In order to develop a full 3D transient heat transfer model, the simplifying assumptions in this study are made as follows:

1) The ground is regarded as a homogeneous medium with mean thermal physical properties.
2) Initial soil surface temperature is assumed as the undisturbed ground surface temperature.
3) Heat transfer in the solid region is regarded as pure heat conduction and the effect of groundwater flow is negligible.
4) A profile of velocity in U-tube pipe is uniform.

In terms of the working fluid flow region, energy equations of the inlet and outlet pipes are setup separately because of the different flow directions.

2.1 Mathematical equations

For heat transfer analysis, the EP is classified into two regions: solid and fluid regions.

2.1.1 Energy balance in solid region

The solid region includes soil, grout and pipe, where heat transfer is regarded as 3D transient heat conduction. The soil is divided into one hundred (100) layers in the vertical direction in order to interpret the fluid temperature variation. Therefore, energy balance equation of the soil domain is given as:

$$\rho_{soil} c_{soil} \frac{\partial T_s}{\partial t} = \frac{\partial}{\partial x}(k_{soil} \frac{\partial T_s}{\partial x}) + \frac{\partial}{\partial y}(k_{soil} \frac{\partial T_s}{\partial y}) + \frac{\partial}{\partial z}(k_{soil} \frac{\partial T_s}{\partial z}) \tag{1}$$

Grout as heat transfer medium in EP has high thermal conductivity and storage capacity. Hence, energy balance equation of the backfill material (grout) domain is given as:

$$\rho_{grout} c_{grout} \frac{\partial T_g}{\partial t} = \frac{\partial}{\partial x}(k_{grout} \frac{\partial T_g}{\partial x}) + \frac{\partial}{\partial y}(k_{grout} \frac{\partial T_g}{\partial y}) + \frac{\partial}{\partial z}(k_{grout} \frac{\partial T_g}{\partial z}) \tag{2}$$

Heat transfer through the pipe is treated as pure heat conduction as well, and defined as 3D heat conduction versus time. Thus, the corresponding energy conservation equation can be written as:

$$\rho_{pipe} c_{pipe} \frac{\partial T_p}{\partial t} = \frac{\partial}{\partial x}(k_{pipe} \frac{\partial T_p}{\partial x}) + \frac{\partial}{\partial y}(k_{pipe} \frac{\partial T_p}{\partial y}) + \frac{\partial}{\partial z}(k_{pipe} \frac{\partial T_p}{\partial z}) \tag{3}$$

Where ρ_{soil}, ρ_{grout} and ρ_{pipe} are densities of soil, grout and pipe (kg/m^3) respectively; c_{soil}, c_{grout} and c_{pipe} are thermal capacities of soil, grout and pipe (J/kg·K), respectively; k_{soil}, k_{grout} and k_{pipe} are thermal conductivities of soil, grout and pipe (W/m·K), respectively; T_s, T_g and T_p are temperatures of soil, grout and pipe (°C), respectively; t is time (s).

2.1.2 Energy balance in fluid region

Heat convection occurs between the pipe and working fluid, the average temperature of the upward flow fluid is equal to that of the downward flow fluid, so $V_1= -V_2= (-) V$.

The fluid in the inlet pipe (downward flow) can be modelled as:

$$\rho_{fluid} c_{fluid} \frac{\partial T_{inlet}}{\partial t} + (\rho c v)_f \frac{\partial T_{inlet}}{\partial z} = k_{fluid} \frac{\partial^2 T_{inlet}}{\partial z^2} + b_{ig}(T_{grout} - T_{inlet}) \tag{4}$$

Similarly, the fluid in the outlet pipe (upward flow) is modelled as:

$$\rho_{fluid} c_{fluid} \frac{\partial T_{outlet}}{\partial t} + (\rho c v)_f \frac{\partial T_{outlet}}{\partial z} = k_{fluid} \frac{\partial^2 T_{outlet}}{\partial z^2} + b_{og}(T_{grout} - T_{outlet}) \tag{5}$$

Where, ρ_{fluid} is density of working fluid (kg/m^3); c_{fluid} is thermal capacities of working fluid (J/kg·°C); k_{fluid} is thermal conductivity of working fluid (W/m·K); T_{inlet} and T_{outlet} are inlet and outlet fluid temperatures (°C), respectively; b_{ig} is reciprocal of thermal resistance R_{ig} between inlet pipe and grout (W/m^2·K); and b_{og} is reciprocal of thermal resistance R_{og} between outlet pipe and grout (W/m^2·K).

2.2 Multiple EPs model

The single EP has limited heat transfer capacity, so the EP system is normally designed with multiple piles. One arrangement of multiple EPs is shown in Fig.2, sixteen EPs are installed in rectangular shape. A 3D FVM model using a rectangular coordinate system [39] is applied for the EPs performance assessment. The entire soil volume is discretized and each EP is represented by a square column circumscribed by the borehole radius. The soil and working fluid temperatures within the EPs are worked out simultaneously by using an iterative approach. The simulated region is discretized as a finite number of contiguous non-overlapping cell cubes. A black cube (P point) in Fig.2 (e) is regarded as the control volume and its six neighboring nodes are identified as west, east, south, north, top and bottom in which the corresponding cell faces are denoted by w, e, s, n, t' and b respectively, while φ, ω, j represent a nodal point in direction of x, y and z axes, respectively.

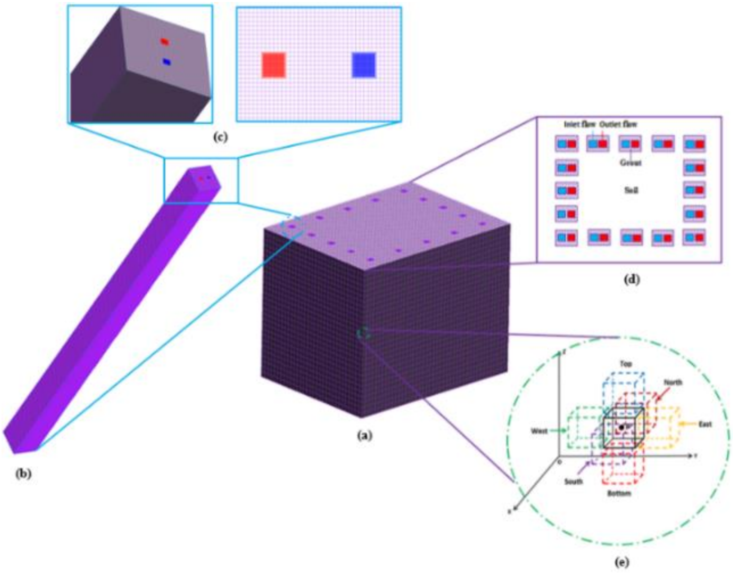

Fig. 2. Schematic diagram of discretised model: (a) 3D multiple EPs model; (b) 3D single EP model; (c) top discretised cross-section of single model; (d) top discretised cross-section of multiple EPs model; (e) arbitrary cube cell [39].

Integration of Eqs. (1) - (5) over the control volume and a time interval from t to (t + Δt) gives

$$\int_{CV}[\int_{t}^{t+\Delta t}\rho c\frac{\partial T}{\partial t}dt]dV=\int_{t}^{t+\Delta t}[(kA\frac{\partial T}{\partial x})_{e}-(kA\frac{\partial T}{\partial x})_{w}]+\int_{t}^{t+\Delta t}[(kA\frac{\partial T}{\partial y})_{n}-(kA\frac{\partial T}{\partial y})_{s}]+\int_{t}^{t+\Delta t}[(kA\frac{\partial T}{\partial z})_{t'}-(kA\frac{\partial T}{\partial z})_{b}] \tag{6}$$

Where, A is surface area of the control volume, CV is its control volume. Thereby, the left side of the volume integral of the temporal derivative can be written as

$$\int_{CV}[\int_{t}^{t+\Delta t}\rho c\frac{\partial T}{\partial t}dt]dV=\rho c(T_{P}-T_{P}^{0})\Delta V \tag{7}$$

Where, $\frac{\partial T}{\partial t}=\frac{1}{\Delta t}(T_{P}-T_{P}^{0})$, this term has been discretised by a first-order (backward) differencing scheme, in which T_{P}^{0} is value of T at time t and T_P is value at time (t+Δt), with Δt is time step, and ΔV=dxdydz.

The fully implicit discretisation method is applied to this proposed model, thereby the value of ε is set equal to 1.

$$I_{T}=\int_{t}^{t+\Delta t}T_{p}dt=[\varepsilon T_{p}+(1-\varepsilon)T_{p}^{0}]\Delta t \tag{8}$$

2.3 Initial and boundary conditions

Cecinato and Loveridge [40] illustrated that the hetero-thermal zone should be accounted for EP design. The ground temperature is a sinusoidal wave function of time and depth, and can be expressed as [41, 42]:

$$T_{soil}(Z, t_{year}) = T_{mean} - T_{amp} \cdot \exp(-Z \times \sqrt{\frac{\pi}{365}}) \cdot \cos[\frac{2\pi}{365} \cdot (t_{year} - t_{shift} - \frac{Z}{2} \times \sqrt{\frac{365}{\pi \cdot \alpha}})] \tag{9}$$

Where T_{soil} (Z, t_{year}) is undisturbed ground temperature at time (t) and depth (Z) (°C); T_{mean} is mean surface temperature (average air temperature) (°C); T_{amp} is amplitude of surface temperature [(maximum air temperature – minimum air temperature)/2] (°C); Z is depth below the surface (surface=0) (m); α is thermal diffusivity of soil (m^2/day); t_{year} is current time (day); t_{shift} is day of the year when the coldest air temperature occurs (day).

Boundary conditions are classified into two categories, the first is expressed in terms of temperature at the boundary while the second is presented in terms of temperature gradient. In the case of the first boundary condition, at z = 0, the inlet pipe temperature is equal to the fluid temperature:

$$T_{inlet}(0, t) = T_{fluid}(t) \tag{10}$$

In terms of the second boundary condition, at z = 0, heat flux at the exit of outlet pipe is depicted as:

$$\frac{\partial T_{outlet}(0, t)}{\partial z} = 0 \tag{11}$$

2.4 COPs of heat pump

A vapour-compression heat pump model is used in this study and its parametric model reflecting the effect of compressor rotation speed is adopted [43].

$$m_r = V_c \omega \rho_{r,suc} \cdot [1 + C_v (1 - \frac{P_{r,cond}}{P_{r,evap}})^{\frac{1}{n}}] \tag{12}$$

$$\Delta\xi_{comp} = \xi_{r,dis} - \xi_{r,suc} = \frac{n}{n-1} \cdot \frac{P_{r,evap}}{\rho_{r,suc}} \cdot [(\frac{P_{r,cond}}{P_{r,evap}})^{\frac{n-1}{n}} - 1] \tag{13}$$

$$Q_{el} = \frac{m_r \Delta h_{comp}}{\eta_{comp}} \tag{14}$$

Where, m_r is refrigerant mass flow rate (kg/s); V_c is compressor swept volume (m^3); ω is compressor rotational speed (rev/s); $\rho_{r,suc}$ is compressor suction refrigerant density (kg/m^3); C_v is compressor volumetric coefficient, P is pressure (kPa); ξ is specific enthalpy (kJ/kg), n is polytropic compression coefficient; η_{comp} is compressor mechanical efficiency; Δξ is specific enthalpy change (kJ/kg); Q_{el} is electrical energy consumption (kW).

The COPs of heat pump are defined as:

$$COP_h = \frac{Q_{heating}}{Q_{el}} \tag{15}$$

$$COP_c = \frac{Q_{cooling}}{Q_{el}} \tag{16}$$

Where COP_h and COP_c are heating and cooling COPs, respectively, $Q_{heating}$ and $Q_{cooling}$ are heating and cooling capacities (kW), respectively.

3 Methodology

3.1 Building and soil property

The numerical model is used to investigate a GSHP performance in a two-storey residential building in the UK. The building with the total floor area of 144 m^2 is designed for one family of four persons, and its monthly heating and cooling energy requirements are shown in Fig.3 [44]. The maximum heating energy is 366 MJ, while the minimum is 128 MJ. By contrast, the maximum cooling energy is 173 MJ and the minimum is 110 MJ.

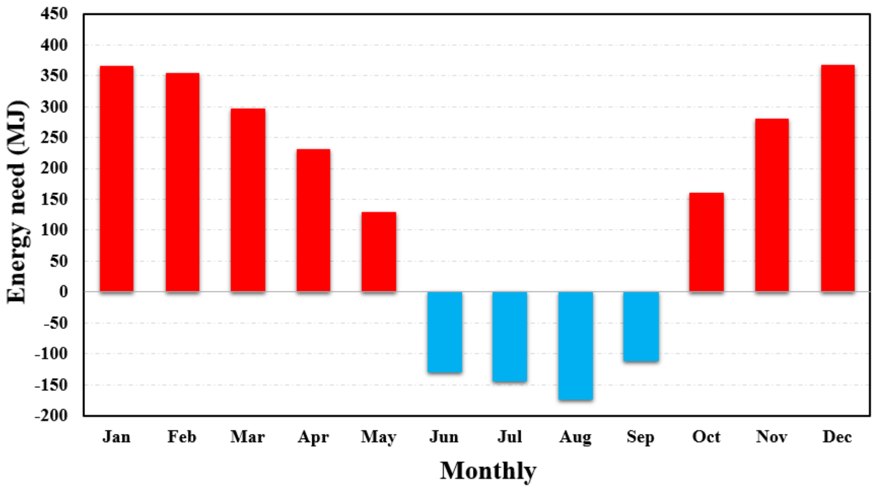

Fig. 3. Monthly heating and cooling energy requirements.

As shown in Fig. 4, the ground consists of four geological layers: (1) the first layer, 0~2.22 m, is made of slightly sandy clay, light grey and very sandy slightly clay gravel; (2) the second layer, 2.22~3.3 m, consists of orange brown mottled grey black and coarse gravel; (3) the third layer, 3.33~5.5 m, is only very soft, red brown, slightly gravel; and (4) the forth layer, 5.5~10 m, is formed with very soft, red brown, slightly gravel clay.

Profile	Depth	Material categories	Thermal conductivity	Density
	0~2.22m	Mixed gravel and coarse sand	1.30 W/(m·K)	2277 kg/m^3
	2.22~3.3m	Sand gravel	1.15 W/(m·K)	2094 kg/m^3
	3.3~5.5m	Slightly Gravel	1.68 W/(m·K)	2223 kg/m^3
	5.5~10m	Slightly Gravel Clay	1.75 W/(m·K)	2392 kg/m^3
	Weighted average		1.5 W/(m·K)	2260 kg/m^3

Fig. 4. The profile of the geological layers within a depth of 10 m [44].

3.2 Multiple EPs system

Total 16 EPs are utilized in this study and arranged in rectangular shape as shown in Fig. 2, the working fluid is a mixture of glycol and water. Table 1 gives the EP parameters [44, 45].

Table 1 Characteristics of the EPs in the experimental system.

Description	Value
Fluid density	1035 kg/m^3
Fluid kinematic viscosity	4.94x10^{-6} m^2/s
Fluid heat capacity	3795 J/(kg ·K)
Fluid thermal conductivity	0.58 W/(m·K)
Pipe density	950 kg/m^3
Pipe heat capacity	2300 J/(kg ·K)
Pipe outside diameter	0.032 m
Pipe inside diameter	0.013 m
Shank spacing	0.06 m
Grout thermal conductivity	2 W/(m ·K)
Grout density	1860 kg/m^3
Grout heat capacity	840 J/(kg ·K)
EP diameter	0.3 m
EP depth	10 m

3.3 Heat pump unit

The EPs are connected to a 5.9 kW Greenline HT Plus heat pump [44, 45] which produces hot water at a temperature range of 35 °C to 65 °C. Table 2 presents technical data of the Greenline HT Plus [46]. The indoor air temperature is used to control the heat pump unit operation, and the set-points are 18 °C and 27 °C for heating and cooling respectively. The main parameters of the initial condition are shown in Table 3.

Table 2 Nominal specification of the heat pump [44].

Description	Value
Emitted /Supplied output at 0/35°C	5.9/1.3 kW
Emitted /Supplied output at 0/50°C	5.4/1.7 kW
Minimum flow heating medium	0.14 l/s
Nominal flow heating medium	0.20 l/s
Superheat	3 °C
Subcooling	4 °C
Refrigerant R407C mass flow rate	0.02 kg/s
Evaporating temperature (dew point)	-1 °C
Condensing temperature (dew point)	58.9 °C
Evaporating pressure	4.5 bar
Condensing pressure	24.7 bar

Table 3 Initial condition and basic parameters.

Description	Value
Initial ground surface temperature	10.4 °C
Soil body temperature (soil far field boundary)	15.0 °C
Soil bottom temperature	15.5 °C
Fluid inlet temperature	1.2 °C

3.4 Simulation program

The year-round operation process is divided into four periods according to the local climate conditions. The first is heating period from 05th/November/2007 to 30th/April/2008, the second is the first soil temperature natural recovery period from 1st/May/2008 to 15th/June/2008, the third is cooling period from 16th/June/2008 to 15th/September/2008, and the last one is the second soil temperature natural recovery period from 16th/September/2008 to 4th/ November /2008. The flowchart of simulation program is presented in Fig.5. The nodal temperature in the equivalent cube is calculated at each step until the time required for the fluid to flow through the pile heat exchangers is reached. The related parameters including temperatures and heat transfer rates are obtained in the process. After that, the program will output the simulation data if the results meet the precision requirement and stop, otherwise the time t will be iterated ($t = t + \Delta t$) and the simulation process starts again.

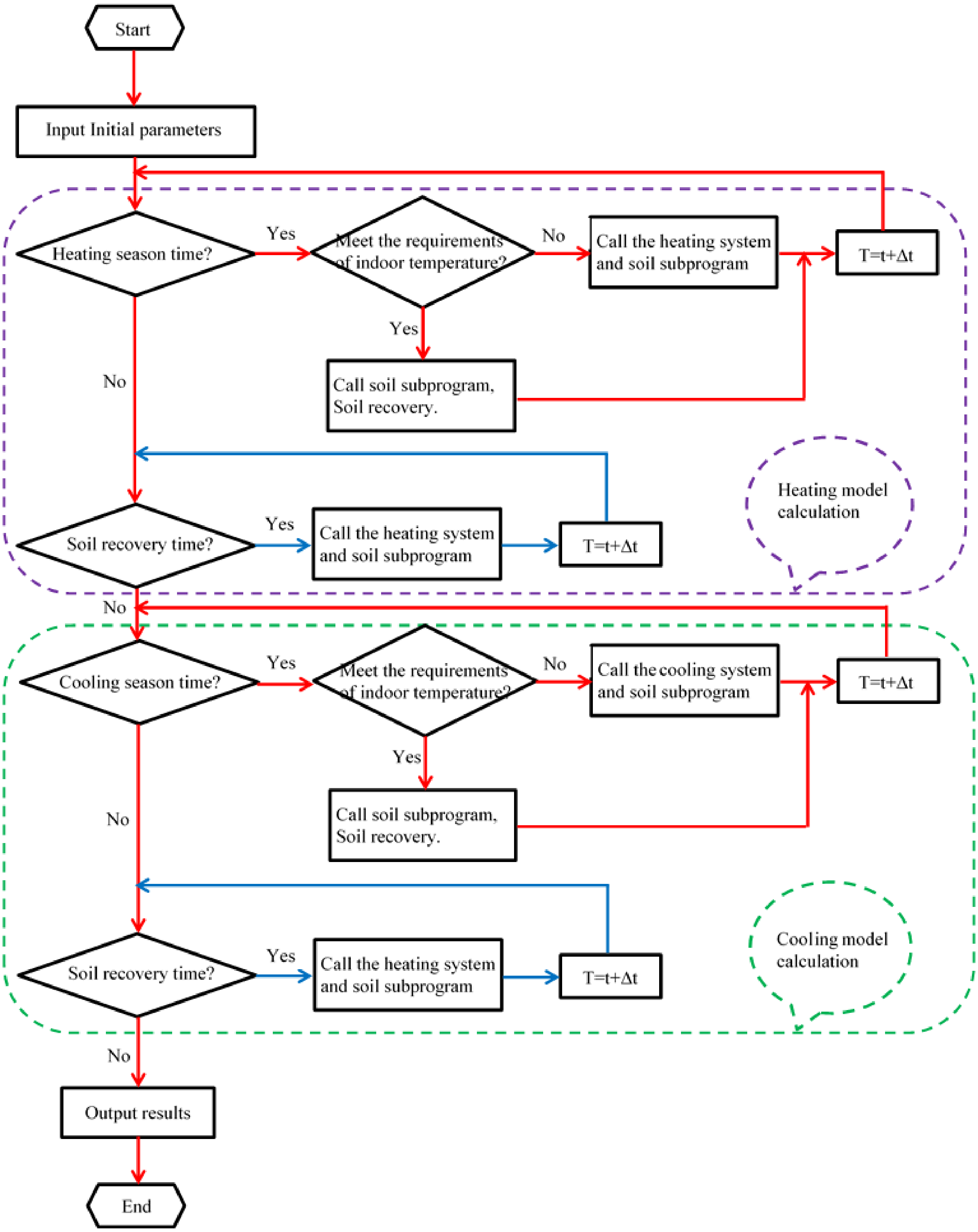

Fig. 5. Flowchart of year-round performance simulation program.

4 Results and discussion

Before the numerical model is utilized to simulate the system performance, it needs to be validated at first. As mentioned in the previous paper [50], the numerical model has been verified by experimental data with less than 8% error. To further validate the numerical model, the experimental data of the heat pump unit in literature [46] are adopted, which are available from November/2007 to May/2008. Fig.6 illustrates the COP_h comparison between the numerical results and experimental data in heating mode, the maximum error is 7.14 % noticed at the beginning of operating stage, and the average error is 6.34 %, thereby the simulation results are effectively supported by the experimental data. Therefore, the 3D numerical model can be utilized to study the annual energy performance of the GSHP with multiple EPs.

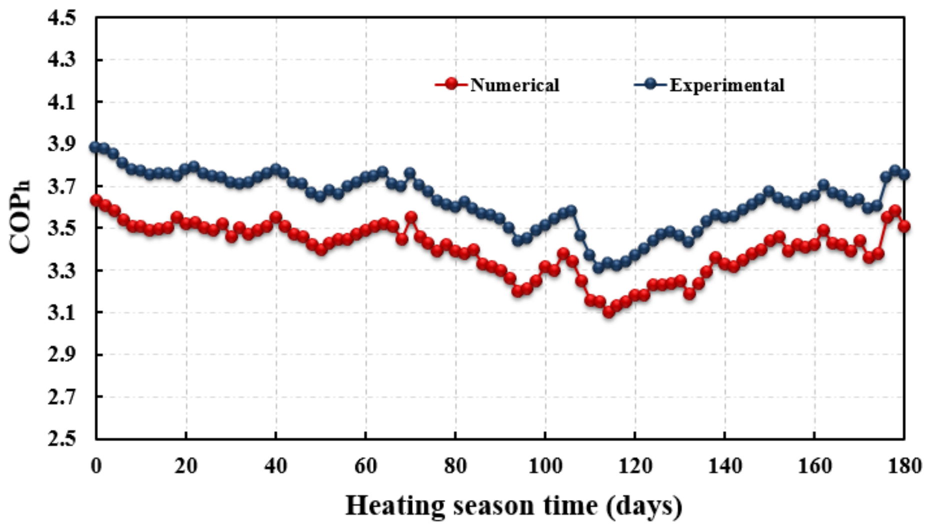

Fig. 6. COP_h of the heat pump.

4.1 Heating period in the first year operation

The system heating performance is simulated and presented in Fig. 7. As can be seen from this figure, the system is capable of meeting the building heating energy demand referring to Fig.3, the system daily thermal energy outputs are lower during the first and last few days than those in the middle period. Notably, the system maximum daily thermal energy output is approximately 2037 MJ on the 116th day, and the minimum value is around 185 MJ on the 172nd day. The building daily internal mean temperatures are shown in Fig.8, it is found that the average temperature of 18.9 °C in heating period is higher than the set value of 18 °C. On the other hand, during the middle period of heating season, the system runs in the most of time so that the ground has no sufficient time to recover. Hence, the ground temperature surrounding the EPs is relatively low, which leads to a low temperature working fluid flowing into the heat pump evaporator, correspondingly a low COP. The maximum value of daily heat extracted from the soil is approximately 1382 MJ on the 116th day, and the minimum value is about 129.8 MJ on the 172nd day.

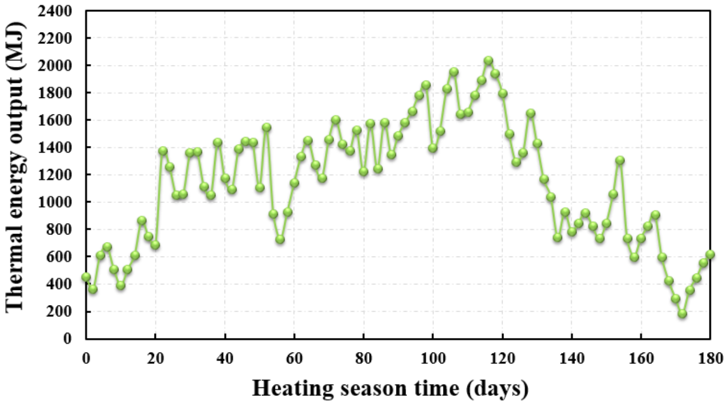

Fig. 7. Daily variations of thermal energy output in heating period.

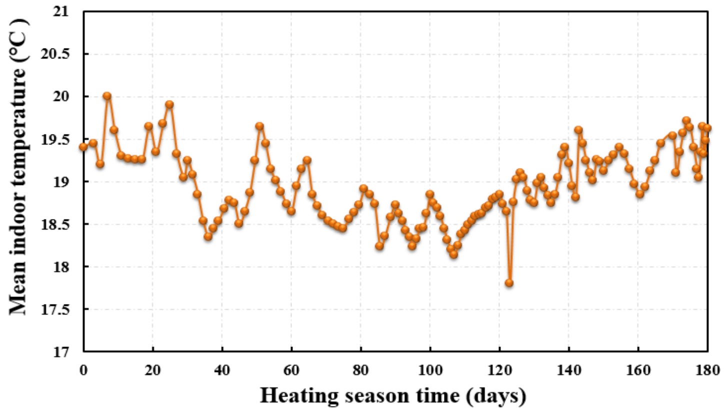

Fig. 8. Daily variation of mean internal temperature in heating period.

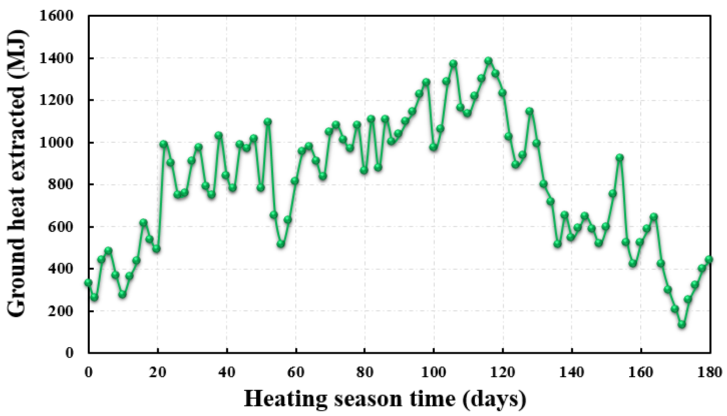

Fig. 9. Daily variation of ground heat extracted in heating period.

4.2 Cooling period in the first year operation

The GSHP is able to meet the building cooling energy requirement (referring to Fig.3) throughout the first year operation period. As shown in Fig. 10, the system maximum daily cooling output is approximately 712 MJ on the 54th day, while the minimum is about 22.6 MJ on the 63rd day. Typically, the indoor temperature fluctuates within an acceptable range during the system operation period as indicated in Fig. 11, it is found that the average indoor temperature of 25.4 °C in cooling period is lower than the set value of 27 °C because the system cooling output is larger than the building cooling load. Fig.12 descripts the daily variation of heat rejected into the ground. The maximum rejected heat is approximately 865.4 MJ on the 54th day, while the minimum value is about 27.5 MJ on the 63rd day.

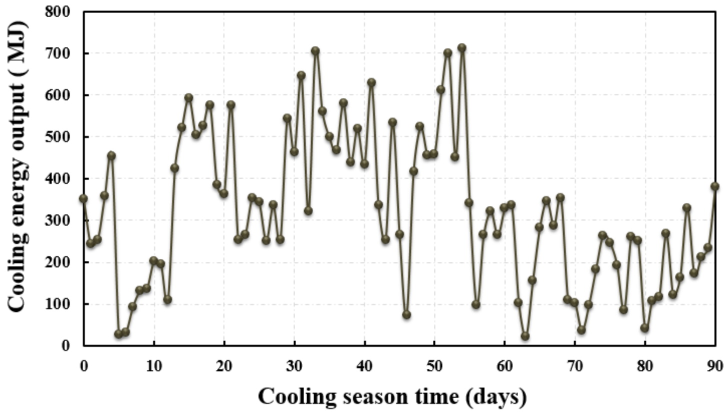

Fig. 10. Daily variations of cooling energy output.

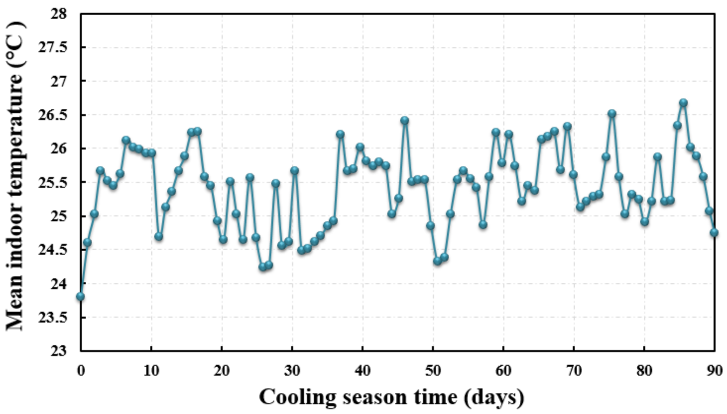

Fig. 11. Daily variations of internal temperature in cooling period.

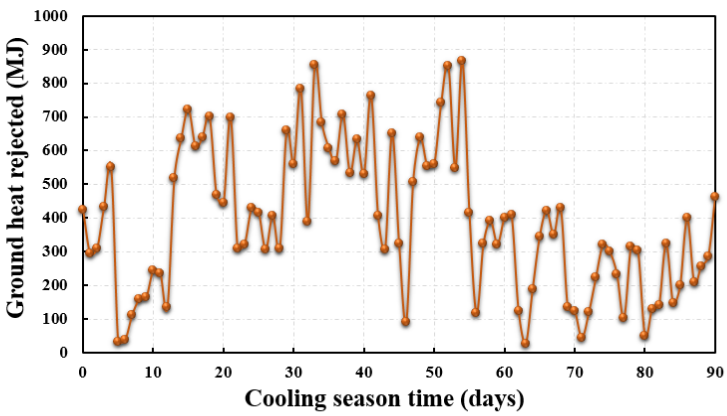

Fig. 12. Daily variations of ground heat rejected in cooling period.

4.3 Soil temperature in the first year operation

In this study, there are two periods used for soil natural recovery as mentioned in Section 3.4. The regression equation developed by Shang et al. [49] is adopted for predicting the soil temperature variation under natural recovery condition. The variations of soil temperature nearby the EPs (soil temperatures in all the diagrams are at 5 m depth underground) throughout the year are illustrated in Fig.13.

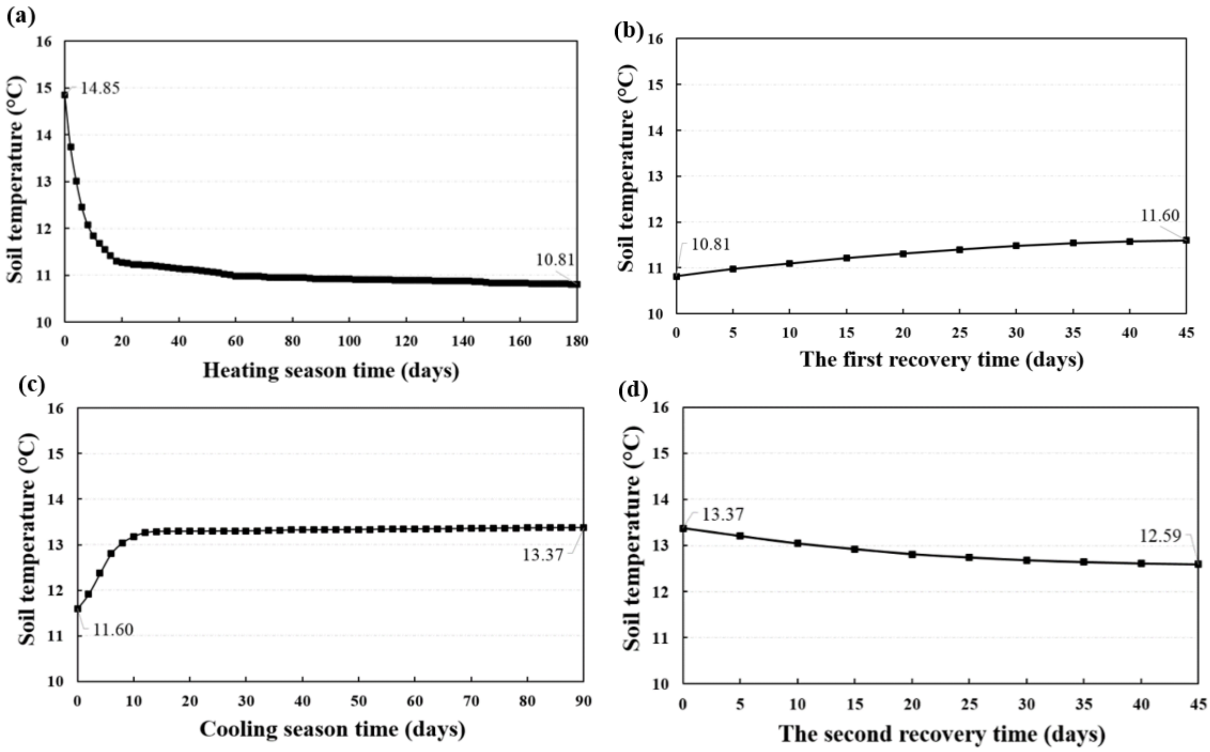

Fig. 13. Daily variations of soil temperature: (a) heating period; (b) the first soil natural recovery period; (c) cooling period; (d) the second soil natural recovery period.

The soil temperature decreases from 14.85 °C at the start to 10.81 °C in the heat extraction period, while it increases from 10.81 °C to 11.60 °C in the first soil natural recovery period. In terms of the heat rejection period, it can be seen that the soil temperature has a dramatically increase from 11.60 °C to 13.37 °C. In the subsequent period, the soil temperature decreases slowly from 13.37 °C to 12.59 °C. The final soil temperature of 12.59 °C is reached which is below its initial temperature of 14.85 °C as expected, therefore the soil has no ability to recover by itself due to the building unbalanced heating and cooling loads.

4.4 Heat pump electricity consumptions and COPs in the first year operation

Fig. 14 depicts electricity consumptions of GSHP unit during heating and cooling periods in the first year operation. It can be seen that electricity consumption gradually reduces when the heating/cooling load drops (referring to Fig. 3). The maximum daily electricity consumption in the heating period reaches approximately 665 MJ, the mean being 450 MJ, while the minimum is about 55 MJ. Obviously, the consumption in the cooling period is far lower than that in the heating periods, the maximum value of electricity consumption is only around 153 MJ on the 54th day, the mean being 70 MJ, while the minimum is about 4.9 MJ on the 63rd day.

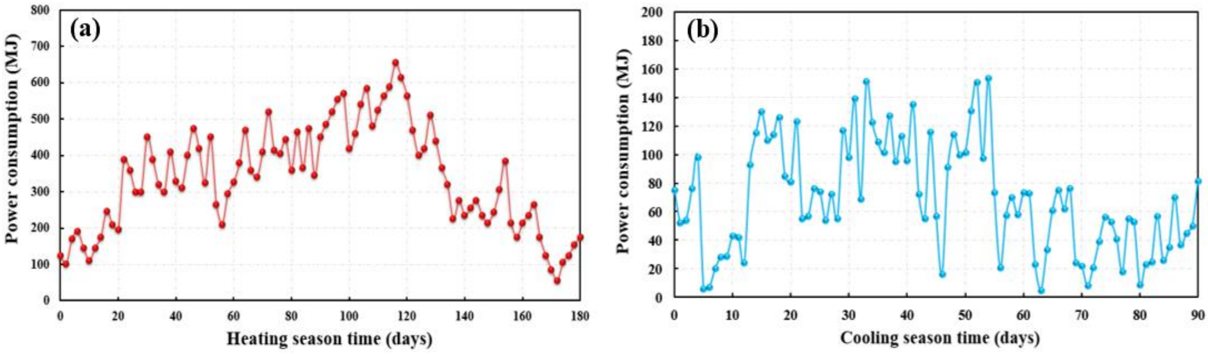

Fig. 14. (a) Power consumption variation in heating period; (b) Power consumption variation in cooling period.

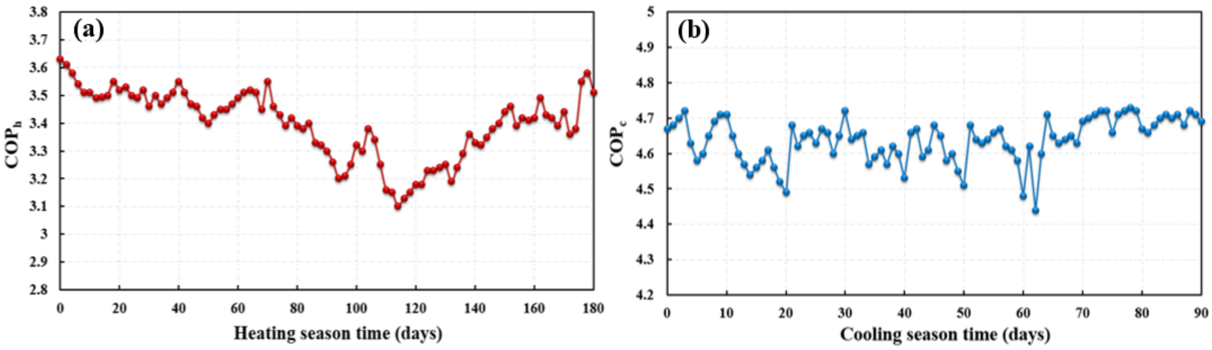

Fig. 15. Daily variations of COPs in the first year: (a) heating period; (b) cooling period.

The COP variations in the heating and cooling periods are described in Fig.15. The maximum value of COP_h is approximately 3.63, the average being 3.41, while the minimum reaches around 3.11. By contrast, the maximum value of COP_c is approximately 4.73, the average being 4.64, while the minimum is around 4.44. Some previous studies have presented the similar COP variations. For example, the seasonal COP_h of a GSHP in Venice, Italy, is 4 and its COP_c is 4.2 in literature [21]. Additionally, the COP range of 3.85 to 4.20 is achieved by a GSHP system in Hong Kong [50]. The monthly COP is investigated through experiment in literature [51], the mean values of 3.03 and 4.33 are presented for heating and cooling respectively.

4.5 Performance in the tenth year

Fig.16 illustrates the system mean heating and cooling energy outputs for the tenth year operation. Notably, the system is still capable of meeting the building heating and cooling requirements. In order to make the soil full recovery, the extra energy should be provided, for example, hot water from a solar collector can be circulated through the EPs to recharge the ground, thereby ameliorating the whole system performance. Fig.17 presents the COP variations for the tenth year operation. The maximum COP_h over the heating period is approximately 3.21, the average being 2.82, while the minimum reaches around 2.47. By contrast, the maximum COP_c is approximately 4.40, the average being 4.31, while the minimum is around 4.08.

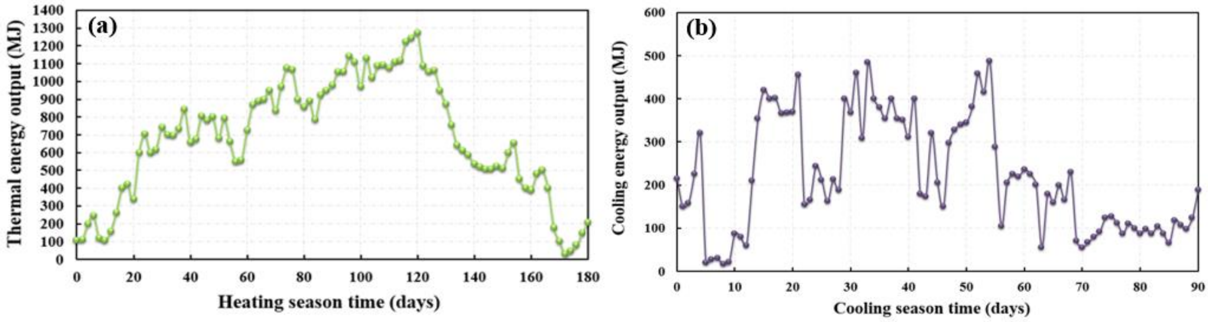

Fig. 16. Daily variations of mean energy output in the tenth year: (a) heating period; (b) cooling period.

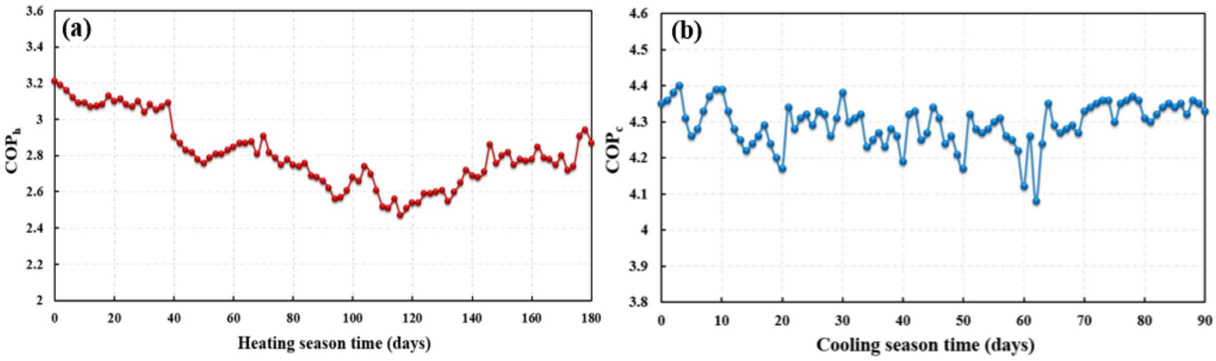

Fig. 17. Daily variations of COPs for the tenth year: (a) heating period; (b) cooling period.

4.6 Influence of soil thermal property

Soil is typically stratified with different materials, including sand, clay, rock and so on. In order to analyze the soil temperature variation surrounding the EPs, gravel, pebbly clay and mild clay are selected as the representatives, their properties, such as volumetric heat capacity, thermal conductivity and diffusivity, are given in Table 4.

Table 4 Soil thermal properties.

Soil type	**Volumetric heat capacity MJ/(m^3·K)**	**Thermal Conductivity W/(m·K)**	**Thermal diffusivity (m^2/s) × 10^{-6}**
Gravel	2.48	1.50 ~1.70	0.50
Pebbly Clay	2.68	1.42	0.73
Mild Clay	3.45	0.96~1.36	0.78

Fig. 18 displays the soil temperature variations surrounding the EPs for the first year operation period. The soil temperature variations have the similar tendencies, and are relatively small. In terms of the mild clay, heat extraction for 180 days brings approximately 4.10 °C temperature decrease (from 14.58 °C to 10.48 °C), while for the pebbly clay, the temperature reduction is around 4.09 °C (from 14.72 °C to 10.63 °C), the similar situation for the gravel, the temperature drops about 4.04 °C (from 14.85 °C to 10.81 °C). During the continuous heat rejection period, the gravel, pebbly clay and mild clay temperatures rise 1.77 °C, 1.74 °C and 1.67 °C, respectively. As for the first natural soil recovery period, it can be seen from Fig.18 (b) that the gravel, pebbly clay and mild clay temperatures increase 0.79 °C, 0.74 °C and 0.72 °C respectively. By contrast, during the second natural soil recovery period, their temperatures decrease 0.77 °C, 0.79 °C and 0.82 °C individually. When the first year operation is completed, the gravel, pebbly clay and mild clay temperatures decrease 2.26 °C, 2.27 °C and 2.3°C respectively compared with their initial temperatures. It is found that the gravel with relatively low volumetric heat capacity and high thermal diffusivity makes thermal energy migrate quickly, and the mid clay with low thermal conductivity and high volumetric heat capacity can store more energy. As a result, it can be deduced that the soil with high thermal conductivity and low volumetric heat capacity has the ability to recover quickly.

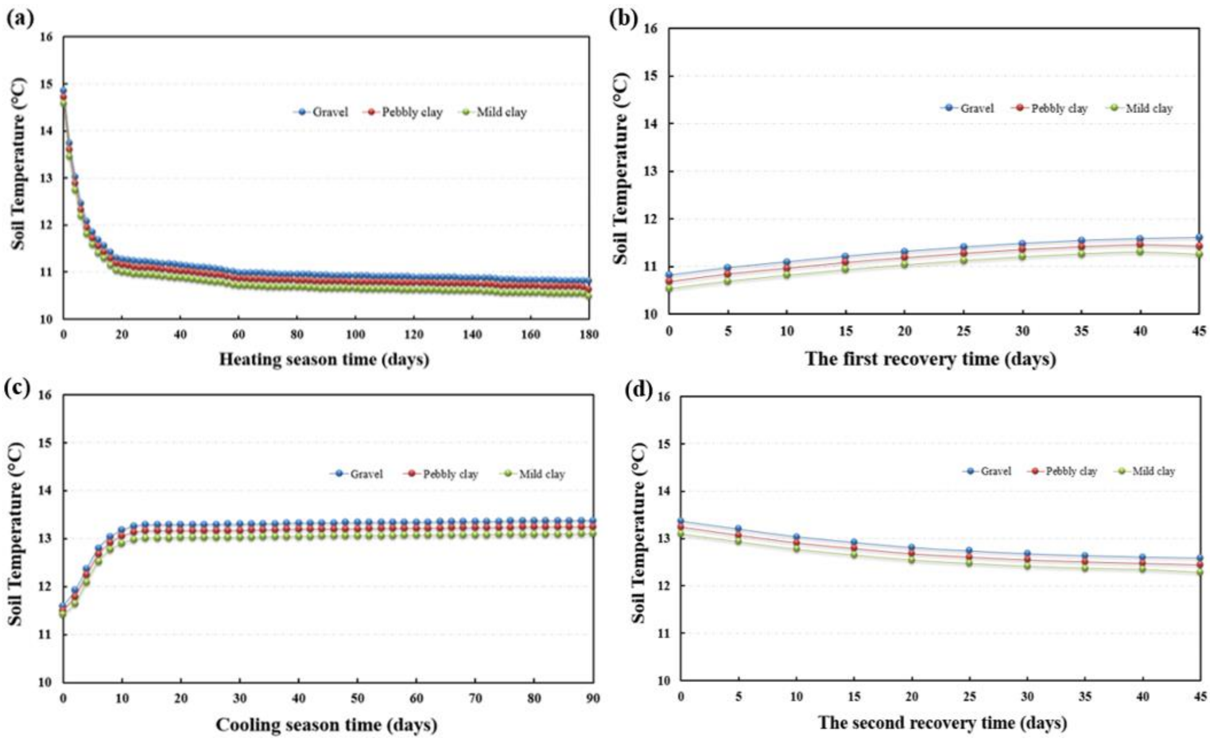

Fig. 18. Soil temperature variations in mild clay, pebbly clay and gravel for the first year operation.

Fig.19 presents the mean soil temperature variations in the tenth year operation. The gravel, pebbly clay and mild clay temperatures decrease 4.02 °C, 4.05 °C and 4.07 °C respectively in the heat extraction period. For the heat rejection period, the soil temperatures of the three soil types rise 1.77 °C, 1.83 °C and 1.89 °C individually. As for the two natural soil recovery periods, the gravel, pebbly clay and mild clay temperatures rise 0.79 °C, 0.73 °C and 0.68 °C respectively at the end of the first period, while at the end of the second recovery period, their temperatures reduce 2.25 °C, 2.26 °C and 2.29°C individually. Finally, the gravel, pebbly clay and mild clay temperatures could reach 7.92 °C, 7.73 °C and 7.50 °C individually at the end of the tenth year operation. Fig. 20

gives the mean COPs of the first year and tenth year operations, it can be seen that the tenth year COP_h, in terms of the mild clay, pebbly clay and gravel, reduce 19.28%, 18.64% and 17.30% respectively compared with that of the first year's. Similarly, the tenth year COP_c reduce 9.17%, 8.37% and 7.11% individually for the three soil types. This is because the soil is not capable of recovering by itself. As a result, the auxiliary system, such as solar collector, has to be adopted to charge the ground in this case.

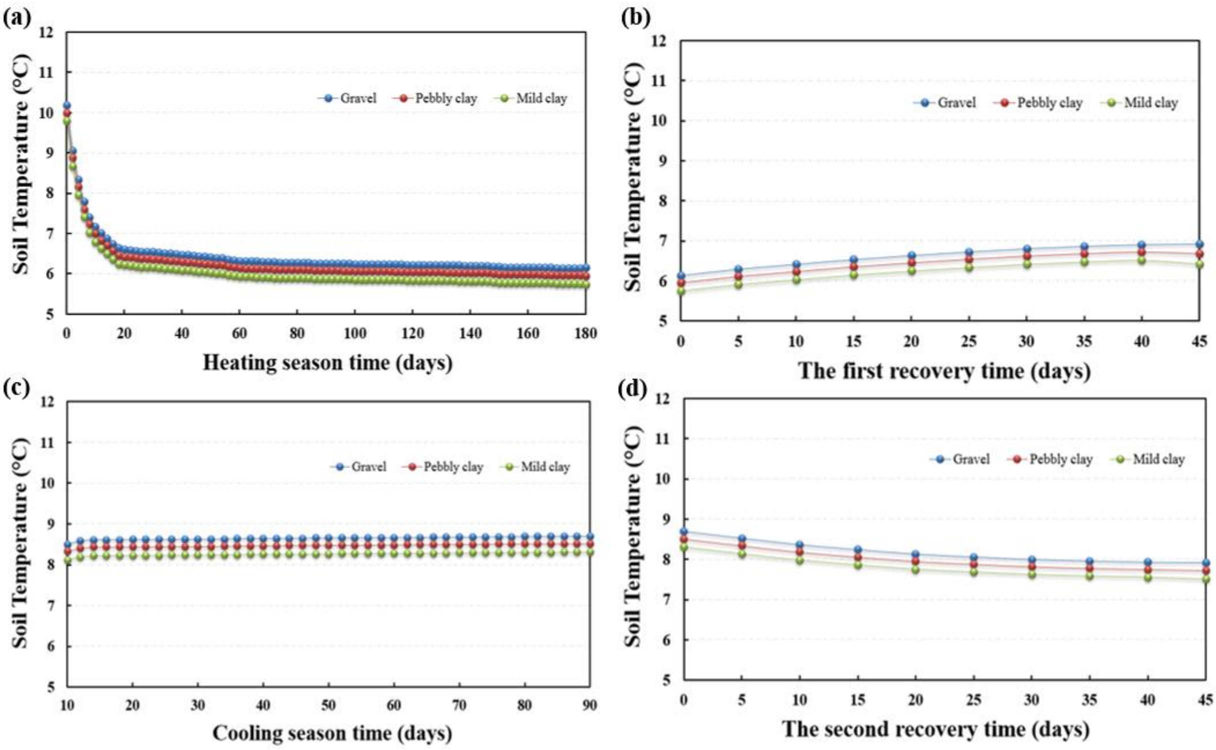

Fig. 19. Soil temperature variation in mild clay, pebbly clay and gravel in the tenth year operation.

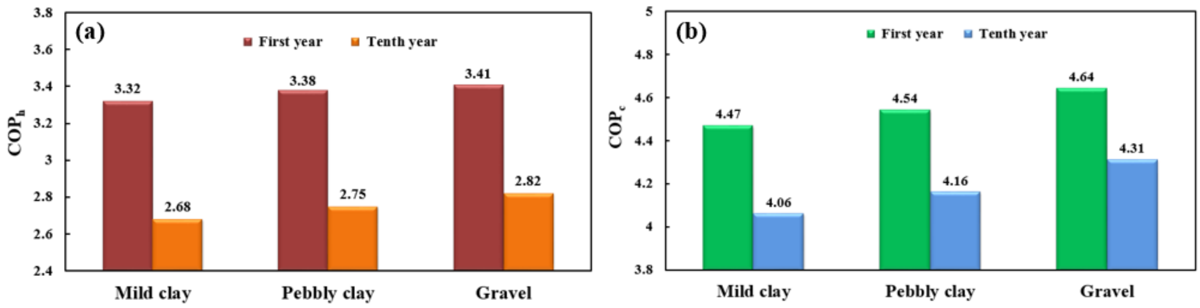

Fig. 20. COP comparisons between the first year and tenth year operations: (a) heating; (b) cooling.

5 Conclusions

The year-round performance of a GSHP with multiple EPs system is simulated through a 3D transient heat transfer numerical model. Sixteen concrete piles are utilized for heat exchange with soil in this study, which have a depth of 10 m. A 5.9 kW nominal heat pump is connected with the EPs, which is used to provide heating and cooling for a typical low-energy home. The soil temperature variations under different operation conditions are investigated as well. The following conclusions are obtained:

(1) In the first year operation, the maximum heat output of the heat pump is 2037 MJ while the minimum is 185 MJ, and the maximum cooling output is 712 MJ and the minimum is 22.6 MJ.

(2) The maximum heat extraction from the ground is 1382 MJ in the first year operation while the minimum is 129.8 MJ, and the maximum heat rejection into the ground is 865.4 MJ and the minimum is 27.5 MJ.

(3) The soil is not capable of recovering by itself because of the building unbalanced heating and cooling loads.

(4) The maximum electricity consumption reaches 665 MJ in the first year heating period, while the maximum electricity consumption in the first year cooling period is only 153 MJ.

(5) In the first year operation, the maximum COP_h is 3.63, the average being 3.40, and the minimum is 3.11; the maximum COP_c is 4.73, the average being 4.63, and the minimum reaches 4.44. By contrast, in the tenth year operation, the maximum COP_h is 3.21, the average being 3.82, and the minimum is 2.47; the maximum COP_c reaches 4.40, the average being 4.31, while the minimum is 4.08.

(6) The soil temperature order from high to low is gravel, pebbly clay and mild clay at the end of the first year operation. So the soil with high thermal conductivity and low volumetric heat capacity is more easily recovered.

(7) The system tenth year performance is lower than the first year's, and its mean COP_h decrease 19.28%, 18.64% and 17.30% respectively for the gravel, pebbly clay and mild clay, while its average COP_c reduce 9.17%, 8.37% and 7.11% individually.

For the future research work, the effect of groundwater advection on the soil temperature will be investigated.

References

[1] C.G. Olgun, T. Ozudogru, S. Abdelaziz, A. Senol, Long-term performance of heat exchanger piles, Acta Geotechnica 10 (2015) 553–569.

[2] G. Mihalakakou, M. Santamouris, D.N. Asimakopoulos, A. Argiriou, On the ground temperature below buildings, Solar Energy 55 (1995) 355–362.

[3] S. Zoras, A. Dimoudi, P. Kosmopoulos, Analysis of conductive temperature variation due to multi-room underground interaction, Energy and Buildings 55 (2012) 433–438.

[4] F. Droulia, S. Lykoudis, I. Tsiros, N. Alvertos, E. Akylas, I. Garofalakis, Ground temperature estimations using simplified analytical and semi-empirical approaches, Solar Energy 83 (2009) 211–219.

[5] E.A. Elias, R. Cichota, H.H. Torriani, Q.D.J.V. Lier, Analytical soil-temperature models: correction for temporal variation of daily amplitude, Soil Science Society of America Journal 68 (2004) 784–788.

[6] D. Zheng, E. R.H.Jr, S.W.Running, A daily soil temperature model based on air temperature and precipitation for continental applications, Climate Research 2 (1993) 183–191.

[7] M. Hajmohammadi, M. Moulod, O. Shariatzadeh, S.S. Nourazar, Essential reformulations for optimization of highly conductive inserts embedded into a rectangular chip exposed to a uniform heat flux, Journal of Mechanical Engineering Science 228 (2014)2337–2346.

[8] M. Hajmohammadi, S. Poozesh, M. Rahmani, Heat transfer improvement due to the imposition of non-uniform wall heating for in-tube laminar forced convection, Applied Thermal Engineering 61 (2013) 268–277.

[9] M. Hajmohammadi, A. Campo, S. Nourazar, Improvement of forced convection cooling due to the attachment of heat sources to a conducting thick plate, Journal of Heat Transfer 135 (2013) 124504–124511.

[10] M. Li, A.C.K. Lai, Heat-source solutions to heat conduction in anisotropic media with application to pile and borehole ground heat exchangers, Applied Energy 96 (2012) 451–458.

[11] A. Casasso, R. Sethi, Efficiency of closed loop geothermal heat pumps: a sensitivity analysis, Renewable Energy 62 (2014) 737-746.

[12] Lee CK, Effects of multiple ground layers on thermal response test analysis and ground-source heat pump simulation, Applied Energy 88 (2011) 4405–4410.

[13] X. Moch, M. Palomares, F. Claudon, B. Souyri, B.Stutz, Geothermal helical heat exchangers: coupling with a reversible heat pump in Western Europe, Applied Thermal Engineering 81 (2015) 368-375.

[14] Al-Khoury R, Bonnier PG, Brinkgreve, RBJ. Efficient finite element formulation for geothermal heating systems. Part I: steady state. International Journal for Numerical Methods in Engineering 63 (2005) 988–1013.

[15] Al-Khoury R, Bonnier PG. Efficient finite element formulation for geothermal heating system. Part II: transient. International Journal for Numerical Methods in Engineering 67 (2006) 725–745.

[16] Al-Khoury R, Kolbel T, Schramedei R. Efficient numerical modelling of borehole heat exchangers. Computers and Geosciences 36 (2010) 1301–1315.

[17] T.Y. Ozudogrua, C.G.Olgunb, A.Senola, 3D numerical modelling of vertical geothermal heat exchangers, Geothermics 51(2014)312–324.

[18] P. Bayer, D. Saner, S. Bolay, L. Rybach, P. Blum, Greenhouse gas emission savings of ground source heat pump systems in Europe: a review, Renewable & Sustainable Energy Review 16 (2012)1256–1267.

[19] M. Li, A.C.K. Lai, Thermodynamic optimization of ground heat exchangers with single U-tube by entropy generation minimization method, Energy Conversion and Management 65 (2013) 133–139.

[20] R. Saggu, T. Chakraborty, Thermal analysis of energy piles in sand, Geomechanics and Geoengineering 10 (2015) 10-29.

[21] N. Batini, A.F.R. Loria, P. Conti, D. Testi, W. Grassi, L. Laloui, Energy and geotechnical behaviour of energy piles for different design solutions, Applied Thermal Engineering 86 (2015) 199-213.

[22] F. Dupray, L. Laloui, A. Kazangba, Numerical analysis of seasonal heat storage in an energy pile foundation, Computers and Geotechnics 55 (2014) 67–77.

[23] A.A. Mehrizi, S. Porkhial, B. Bezyan, H. Lotfizadeh, Energy pile foundation simulation for different configurations of ground source heat exchanger, International Communications in Heat and Mass Transfer 70 (2016) 105–114.

[24] T.V. Bandos, A. Campos-Celador, L.M. Lopez-Gonzalez, J.M. Sala-Lizarraga, Finite cylinder-source model for energy pile heat exchangers: Effects of thermal storage and vertical temperature variations, Energy 78 (2014) 639-648.

[25] E. H. N. Gashti, V.-M. Uotinen, K. Kujala. Numerical modelling of thermal regimes in steel energy pile foundations: A case study, Energy and Buildings, 69 (2014) 165-174.

[26] X. Li, Y. Chen, Z. Chen, J. Zhao, Thermal performances of different types of underground heat exchangers, Energy and Buildings 38 (2006) 543–547.

[27] A. Capozza, A. Zarrella, M. D. Carli, Long-term analysis of two GSHP systems using validated numerical models and proposals to optimize the operating parameters. Energy and Buildings 93 (2015) 50–64.

[28] J. Kim, J.C. Jang, E.C. Kang, K.C. Chang, E.J. Lee, Y. Kim, Verification study of a GSHP system manufacturer data based modeling, Renewable Energy 54 (2013) 55–62.

[29] J. Darkwa, W. Su, D.H.C. Chow, Heat dissipation effect on a borehole heat exchanger coupled with a heat pump, Applied Thermal Engineering 60 (2013) 234–241.

[30] P. Pasquier, D. Marcotte, Joint use of quasi-3D response model and spectral method to simulate borehole heat exchanger, Geothermics 51 (2014) 281–299.

[31] W. Retkowski, J. Thöming, Thermo-economic optimization of vertical ground-source heat pump systems through nonlinear integer programming, Applied Energy 114 (2014) 492–503.

[32] J.S. Lee, H. Park, Y. Kim, Transient performance characteristics of a hybrid ground source heat pump in the cooling mode, Applied Energy 123 (2014)121–128.

[33] T. Kurevija, D. Vulin, V. Krapec, Effect of borehole array geometry and thermal interferences on geothermal heat pump system. Energy Convers Manage 60 (2012) 134–42.

[34] R. Ghoubali, P. Byrne, J. Miriel, F. Bazantay, Simulation study of a heat pump for simultaneous heating and cooling coupled to buildings, Energy and Buildings 72 (2014) 141–149.

[35] O.Kizilkan, I.Dincer, Borehole thermal energy storage system for heating applications: thermodynamic performance assessment, Energy Conversion and Management 90 (2015) 53–61.

[36] Q. Zhao, B.M. Chen, F. Liu, Study on the thermal performance of several types of energy pile ground heat exchangers: U-shaped, W-shaped and spiral-shaped, Energy and Buildings 133 (2016) 335–344.

[37] J. Luo, H.F. Zhao, S.Q. Gui, W. Xiang, J. Rohn, P. Blum, Thermo-economic analysis of four different types of ground heat exchangers in energy piles, Applied Thermal Engineering 108 (2016) 11–19.

[38] Y. Hamada, H. Saitoh, M. Nakamura, H. Kubota, K. Ochifuji, Field performance of an energy pile system for space heating, Energy and Buildings 39 (2007) 517–524.

[39] Y. Cui, J. Zhu, 3D transient heat transfer numerical analysis of multiple energy piles, Energy and Buildings 134 (2017) 129–142

[40] F. Cecinato, F.A. Loveridge, Influences on the thermal efficiency of energy piles, Energy 82 (2015) 1021–1033.

[41] G.A. Florides, S.A. Kalogirou, Annual ground temperature measurements at various depths (2004).

[42] T. Kusuda, O. Plet, J.W. Bean, Annual variation of temperature field and heat transfer under heated ground surfaces: slab-on-grade floor heat loss calculations, Centre for Building Technology National Bureau of Standards Washington, DC 20234.

[43] H. Jin, J.D. Spitler, A parameter estimation based model of water-to-water heat pumps for use in energy calculation programs, ASHRAE Transactions 108 (2002) 4493-4510.

[44] C.J. Wood, Investigation of Novel Ground source Heat Pump, in: Built Environment, Vol. Doctor of Philosophy, University of Nottingham, 2009.

[45] C.J. Wood, H. Liu, S.B. Riffat, An investigation of the heat pump performance and ground temperature of a piled foundation heat exchanger system for a residential building, Energy 35 (2010) 4932–4940.

[46] Greenline HT Plus, http://www.intelligentenergysolutions.com/assets/images/Datasheets/Ground_Source Heat Pumps/IE SIVT Green line HTPlus.pdf.

[47] Y. Shang, M. Dong, S.F. Li, Intermittent experimental study of a vertical ground source heat pump system, Applied Energy 136 (2014) 628–635.

[48] C. K. Lee, Effect of borehole short-time-step performance on long-term dynamic simulation of ground-source heat pump system, Energy and Buildings 129 (2016) 238–246.

[49] H. Esen, M. Inalli, Y. Esen, Temperature distributions in boreholes of a vertical ground-coupled heat pump system, Renewable Energy 34 (2009) 2672–2679.

Nomenclature

A	Area (m^2)
b	Reciprocal of thermal resistance
c_p	Heat capacity (J/(kg·K))
d	Diameter (m)
C_v	Volumetric coefficient of compressor
h	Heat transfer coefficient (W/(m^2·K))
H	Height (m)
k	Thermal conductivity (W/m·K)
l	Length (m)
m_r	Refrigerant mass flow rate (kg/s)
n	Polytropic compression coefficient
P	Pressure (kPa)
Q	Energy capacity (kW)
R	Thermal resistance (W/m^2·K)
V_c	Swept volume of compressor (m^3)

Greek Letters

α	Ground thermal diffusivity (m^2/day)
Δd	Shank spacing (m)
Δh	Specific enthalpy change (kJ/kg)
ΔT	Temperature gradient (°C)
Δt	Time interval (s)
Δx, Δy, Δz	Space interval at different directions
η	Efficiency
ρ	Density (kg/m^3)

τ	Period of a temperature cycle (s)
μ	Dynamic viscosity ($N \cdot s/m^2$)
ν	Kinematic viscosity (m^2/s)
δ	Pipe wall thickness of square cross-section pipe (m)
$\rho_{r,suc}$	Compressor suction refrigerant density (kg/m^3)
$\Delta\psi$	Temperature interval (°C)
ω	Rotational speed of compressor (rev/s)
ξ	Specific enthalpy (kJ/kg)
$\Delta\xi$	Specific enthalpy change (kJ/kg)

Subscripts

ave	Average
b	Borehole
c	Compressor
cond	Condenser
el	Electricity
evap	Evaporator
f	Fluid
g	Grout
ig	Inlet pipe and grout
og	Outlet pipe and grout
p	Pipe
s	Soil
v	Vapour
w,e,s,n,b,t'	West, east, south, north, bottom, top
r	Refrigerant

Abbreviations

BHE	Borehole heat exchanger
COP	Coefficient of performance

CV	Control volume
EP	Energy pile
FEM	Finite element method
FVM	Finite volume method
GHE	Ground heat exchanger
GSHP	Ground source heat pump
3D	Three-dimensional